Energy & Environmental Science

Accepted Manuscript

ROYAL SOCIETY OF CHEMISTRY

www.rsc.org/ees

Table of Contents

In ternary blend of P3HT:PCPDTBT:$PC_{61}BM$, bundles of well-defined P3HT fibrils formed a network in a matrix comprised of a mixture of P3HT, PCDTBT and PCBM yielding a 27% improvement in device efficiency.

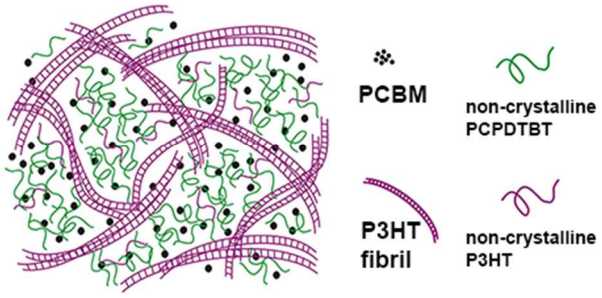

Guided Crystallization of P3HT in Ternary Blend Solar Cell Based on P3HT:PCPDTBT:PCBM

Yu Gu,[a] Cheng Wang,[b] Feng Liu,[a] Jihua Chen,[c] Ondrej E. Dyck,[d] Gerd Duscher,[d]
Thomas P. Russell*[a]

[a] Department of Polymer Science and Engineering, University of Massachusetts-Amherst, Amherst, MA 01003, USA. E-mail: russell@mail.pse.umass.edu
[b] Advanced Light Source, Lawrence Berkeley National Laboratory, Berkeley, CA 94720, USA
[c] Center for Nanophase Materials Sciences, Oak Ridge National Laboratory, Oak Ridge, TN 37831, USA
[d] Department of Materials Science and Engineering, University of Tennessee, Knoxville, TN 37996, USA

To mimic the performance of the tandem solar cells, ternary blend solar cells with a single active layer of P3HT:PCPDTBT:$PC_{61}BM$ were cast from chlorobenzene and thermally annealed. By varying blending ratio, thermal annealing time and P3HT molecular weight, the device performance was enhanced relative to the binary references. To understand this, the morphology of the active layer was studied using hard and soft x-ray scattering methods in concert with bright field and energy resolved transmission electron microscopies. We found that the phase separation of the amorphous PCPDTBT and P3HT guided the formation of P3HT fibrils, resulting in a unique multi-length-scale morphology. This morphology consisted of bundles of well-defined P3HT fibrils, forming a network, imbedded in an amorphous mixture of the PCBM, PCPDTBT and P3HT. The two polymers acted independently in their specific photoactive ranges, and the sensitization of PCPDTBT benefited the cascade charge transfer. This multi-length-scale morphology was linked to the improved device performance of P3HT: PCPDTBT:$PC_{61}BM$ and the photophysics of the active layer.

1. Introduction

To improve the power conversion efficiency (PCE) of organic photovoltaic (OPV) devices, one strategy is to increase the total number of photons absorbed by the components. Achieving this

goal requires the synthesis of new materials or developing processing routes to use two or more existing materials that have complementary absorptions in the solar spectrum. Typically, a tandem-cell geometry is used to achieve this, where two or more sub-cells are stacked together and connected in series or in parallel.[1-3] The highest efficiency to date of 12% for organic solar cells was reported by Heliatek GmbH using this strategy.[4] However, the fabrication of tandem cells is not cost-efficient for large scale production, since this involves a multiple-step layer-by-layer processing, the engineering of cell-connecting layers and the optimization of the sub-cell thickness.[1,5-8] To simplify the processing procedure and achieve the comparable efficiencies as tandem cells, ternary blend can be used as the active layer. Such ternary blend consists of two donor materials active in different wavelength ranges of the solar spectrum with one electron transporting material, such as PCBM.[9,10]

There have been only a few successful ternary blend solar cells reported having improved device performance relative to the binary cells; among them, the ternary blends based on two donor polymers and one fullerene acceptor are even rare.[11-18] The influence of adding a secondary donor material to the host matrix has not been fully understood. The most frequently used ternary mixture combines poly[2,6-(4,4-bis- (2-ethylhexyl)- 4H-cyclopenta [2,1-b;3,4-b'] -dithiophene)-alt-4,7-(2,1,3-benzothiadiazole)] (PCPDTBT) with poly(3-hexylthiophene -2,5-diyl) (P3HT) and [6,6]-phenyl-C_{61}-butyric acid methyl ester ($PC_{61}BM$).[12,13,16,19] Previous studies on this system have focused primarily on device physics. It has been shown that incorporating PCPDTBT into the P3HT:PCBM matrix not only helps to extend the light absorption to the near-infrared region but also bridges the charge transport between P3HT and PCBM, due to the cascade alignment of energies levels.[12,16] In addition, the crystallinity of each component and their miscibilities have

been noted, but morphological studies, which is one of the key factors in determining the overall success of the device, are very limited.[16,19]

Here, we investigated this ternary blend to understand the morphology of ternary blend solar cells. Studies were carried out as a function of the concentration of P3HT and PCPDTBT after spin-coating by chlorobenzene solution and then thermal annealing. The molecular weight of P3HT was varied. Comparisons of the morphologies of the ternary mixture with the corresponding binary mixtures were performed to understand the influence of the third component on the morphologies. Grazing incidence x-ray diffraction (GIXD) and polarized resonant soft x-ray scattering (P-RSoXS) were used in combination with transmission electron microscopy (TEM) to assess the morphology of the active layer, including the ordering and orientation of each component, the degree of phase separation, and spatial distribution of each component. The relationship between the bulk morphology, device performance and the photophysics was developed.

2. Experimental

2.1 Materials

P3HT-32k (M_n=31.5k, M_w=40.9k, PDI=1.3) was synthesized according to the references.[20] P3HT-28k (M_n=28.4k, M_w=33.3k, PDI=1.17) was provided by Kuraray Co. Ltd, Japan. P3HT-19k (M_n=18.6k, M_w=33.5k, PDI=1.8) and [6,6]-phenyl-C_{61}-butyric acid methyl ester ($PC_{61}BM$) was purchased from American Dye Source, Inc. PCPDTBT (M_n=19.2k, M_w=36.5k, PDI=1.9) was purchased from 1-material Chemscitech Inc. (St-Laurent, Quebec, Canada). All of these materials were used as received and dissolved in chlorobenzene. ~130 nm-thick thin films were

prepared by spin-coating the solution on the PEDOT:PSS coated substrates. The thickness was determined by surface profilometer (Alpha Step IQ).

2.2 Device Preparation and Optoelectronic Characterization

Photovoltaic devices were fabricated by the following structure: glass / indium tin oxide (ITO, Thin Film Devices Inc.) / poly(3,4-ethylenedioxythiophene) : polystyrene sulphonate (PEDOT: PSS, CLEVIOS^{TM} P VP Al 4083, ~40 nm) / active layer (~130 nm) / Al (~100 nm). The active area is 6 mm^2. For pre-annealing, the devices were placed directly onto a 150 ^{o}C hot plate and heated before Al deposition; as for post-annealing, the devices were annealed for various times as indicated in the main text with the Al electrodes. All current-voltage (I-V) characteristics of the devices were measured under simulated AM1.5G irradiation (100 mW cm^{-2}) using a Xe lamp-based Newport 91160 300-W Solar Simulator.

2.3 Morphology Characterization

Grazing Incidence X-ray Diffraction (GIXD): Silicon wafers coated with PEDOT:PSS were used as the substrates. Thin-film preparation procedures for GIXD samples were kept the same as for device fabrication. The Al cathode was removed with an aqueous $CuCl_2$ solution. GIXD measurements were performed on beamline 7.3.3 at the Advanced Light Source at the Lawrence Berkeley National Laboratory. The samples were put in the Helium chamber to suppress the air scattering.

Polarized Resonant Soft X-ray Scattering (P-RSoXS) and Near Edge X-ray Absorption Fine Structure (NEXAFS): P-RSoXS and NEXAFS experiments were performed at soft x-ray

scattering beamline 11.0.1.2. at the Advanced Light Source (ALS), LBNL.[21] The thin film samples were floated on the single plot copper grids and measured by transmission geometry.

Transmission Electron Microscopy (TEM): The thin film samples were floated on 400 mesh copper grids. Bright field transmission electron microscopy (BF-TEM) was performed on samples using a JEOL 2000FX electron microscope operated at 200 kV. Energy filtered transmission electron microscopy (EF-TEM) were at the Center for Nanophase Materials Sciences, Oak Ridge National Laboratory. The samples were examined with a Zeiss Libra 120 equipped with an in-column (Omega) energy filter at 120kV. Focused ion beam (FIB) was performed in department of materials science and engineering, University of Tennessee, with a Zeiss Auriga dual beam FIB-SEM (5-30kV). A final polishing at 10pA/10kV was used to minimize ion beam damage during FIB processes and the resultant cross-sectional TEM samples have a thickness of ~70 nm.

Optical microscopy (OM): The thin film samples on PEDOT:PSS coated Si wafers were probed by Olympus BX60 optical microscope in reflection mode.

3. Results and Discussion

Thin films of P3HT:PCPDTBT:$PC_{61}BM$ or their binary references were spin-coated from chlorobenzene (CB), then thermally annealed at 150 ^{o}C for 10 minutes. The thicknesses of the films were kept constant. Figure 1 shows the out-of-plane (OOP) and in-plane (IP) grazing incidence x-ray diffraction (GIXD) profiles of the mixtures as a function of the weight ratio of the two polymers based on P3HT-32k, where the weight ratio of the total polymer to $PC_{61}BM$

was held constant at 1/1. For P3HT:$PC_{61}BM$ thin films (0% PCPDTBT weight fraction), P3HT crystallized after thermal annealing, as evidenced by the appearance of strong OOP (h00) reflections as seen in pure P3HT. (also see Figure S1) The (010) peak of P3HT at q ~1.7 A^{-1} is seen in the OOP profiles and (h00) peak is also seen in the IP profile. These data suggest that a certain degree of face-on orientation was present, though the edge-on orientation dominated.[22,23] The broad peak at ~1.4 A^{-1} is assigned to the form factor of PCBM.[24]

By gradually incorporating PCPDTBT, up to a 25% of weight fraction, the diffraction peaks characteristic of PCPDTBT at q~0.59 A^{-1} were not evident, suggesting that PCPDTBT was amorphous. (Figure 1 and S1) This is consistent with previous studies where the miscibility of PCBM with PCPDTBT can disrupt the chain packing of PCPDTBT.[25-28] The OOP (h00) peaks of P3HT were quite evident and the peak position remained constant. Very little change in the peak intensity was observed. These data indicate that P3HT and PCPDTBT do not co-crystallize. The sizes of the crystals, estimated using the Scherrer equation: $L = 0.9 \lambda / (\beta \cos \theta)$, where λ is the wavelength of the incident beam, β is the full width at half maximum (FWHM) in radians, and θ is the Bragg angle, are given in Figure 1c. As seen, the P3HT crystals do not change significantly with the addition of a small amount of PCPDTBT. In addition, the peak at q~1.7 A^{-1} in the OOP profile was also obvious and its intensity decreased with increasing amounts of PCPDTBT. So this peak was mainly attributed to the (010) reflection of P3HT and not (010) reflection of PCPDTBT. Meanwhile, the intensity of the corresponding peak at q~1.7 A^{-1} in the IP profile increased with increasing PCPDTBT contents. This suggested that the edge-on orientation for P3HT chains increased with the addition of a small amount of PCPDTBT. However, if the concentration of PCPDTBT became too high, the ordering of P3HT was

suppressed. Increasing the weight fraction of PCPDTBT to 50% caused a significant drop in the intensity of the crystalline reflections. Crystalline ordering was completely lost when the PCPDTBT content exceeded 75%. (Figure S1)

The formation of P3HT crystals was confirmed by bright field TEM (BF-TEM) images. Note that the pre-annealed and post-annealed samples showed the same degree of phase separation in the lateral direction, which is demonstrated by BF-TEM images and RSoXS profiles (Figure S2). As seen in Figure S2, the primary difference is that post-annealed samples had wrinkles on the surface, which influenced the focus for TEM imaging. Consequently, the pre-annealed samples are shown to illustrate the detailed features clearly. For the P3HT-32k:$PC_{61}BM$ blend, fine P3HT crystals were observed, as evidenced by the small bright domains. (Figure 2a) The ternary blend of P3HT-32k:PCPDTBT:$PC_{61}BM$ exhibited a rather unique morphology (Figure 2b-f), where bundles of P3HT fibrils (bright areas) formed a continuous network imbedded in a mixture of $PC_{61}BM$ with amorphous PCPDTBT and P3HT (dark areas). The center-to-center distance for the dark areas, or in other words, the bundle-to-bundle distance, increased with the increasing weight fraction of PCPDTBT, up to 25%. When the concentration of PCPDTBT exceeded 50% (Figure 2g), few P3HT fibrils can be seen. And when the PCPDTBT weight fraction exceeded 75%, no evidence of fibrils was found. (Figure 2h-i) The phase separation was suppressed as well when the crystallinity was lost. From these data it is evident that PCBM is miscible with amorphous P3HT and PCDTBT, acting as a common solvent for both polymers.

The spatial distribution of each component was determined by energy filtered TEM (EF-TEM) images, following a previously reported method based on the low eV (15-40eV) plasmon

responses of the polymer donor and fullerene acceptor.[29] The zero-loss mapping (0±4eV) image (Figure 3a) for the ternary blend with 25% PCPDTBT looked similar to the BF-TEM image in Figure 2f. In the 19±4 eV image (Figure 3b), where the energy is characteristic of the polymers, the bright areas were assigned to the polymer-rich regions, particularly P3HT crystals, considering the low concentration of PCPDTBT.[29] Unfortunately, it is impossible to distinguish P3HT from PCPDTBT, because the characteristic plasmon loss peak for P3HT is very close to that for PCPDTBT, as measured in our electron energy loss spectroscopy experiments. In the 30±4 eV image (Figure 3c), where the energy is characteristic of $PC_{61}BM$, the bright areas corresponded to the PCBM-rich regions. The color mix map is shown in Figure 3d, which was generated by highlighting Figure 3b and 3c with red and green colors, respectively, and then overlapping the two images. It indicated that the polymer-rich region and PCBM-rich region are complementary to each other. Based on these results we can schematically represent the morphology as shown in Figure 3e.

A cross-section of the post-annealed sample was prepared using a focused ion beam (FIB), then investigated by EF-TEM. The original images are shown in Figure 3f-h. The color mix map is shown in Figure 3i, where the green color corresponds to PCBM-rich regions and the red color for the polymer-rich regions. It is clear that polymer-rich and PCBM-rich regions are essentially complementary. The domain size in the cross-sectional image is essentially the same as in the lateral direction.

Polarized resonant soft x-ray scattering (P-RSoXS) was also used to probe the morphology of the ternary blend where, by varying the incident x-ray energy to the absorption edges characteristic

of the chemical bonding of different components, the contrast of each component can be changed.[30] Furthermore, since the x-ray beam is polarized, the contrast also depends on the orientation of the bonds with respect to the incident beam.[31] Typical scattering patterns for the annealed P3HT-32k:PCPDTBT thin film with a 3/1 weight ratio and their sector averaged profiles are shown in Figure 4. Here, the transmission geometry was used with the incident beam normal to the film surface and the diffraction vector oriented in the plane of the film. Thus, the appearance of the scattering maximum at q ~ 0.008 A^{-1} indicated that P3HT and PCPDTBT phase separated. Even for a 1:1 blend of regio-random P3HT, an amorphous polymer, and PCPDTBT, a scattering maximum was observed, confirming the immiscibility of P3HT and PCPDTBT. (Figure S3)

The scattering patterns were found to be anisotropic for certain beam energies (Figure 4). A stronger scattered intensity along the horizontal direction was found with a horizontally polarized beam at 284 eV; while the scattering intensity was stronger along the vertical direction at 285.4 eV. The maximum in the scattering occurred at the same scattering vector. It must be noted that the sample was not oriented in-plane; the scattering patterns were independent of the rotation of the sample. The horizontally enhanced pattern would change to vertically enhanced if the polarization of the beam was rotated by 90°. (Figure S4) Consequently, the anisotropy in the pattern originates from a local molecular orientation of each component. The orientation of the C-1s→π*c=c transition dipole moment of the molecule is perpendicular to the conjugation plane.[31,32] When the polarization direction of the beam is parallel to the transition dipole moment, absorption is stronger. According to near edge x-ray absorption fine structure (NEXAFS) profiles for P3HT, PCPDTBT and PCBM (see Figure S5), the carbon K-edge

resonances at 284 eV corresponds to the spectroscopic signature of PCPDTBT and 285.4 eV to P3HT. In Figure 4a and 4b, the direction of the enhancements of scattering patterns are normal to each other when the polarization of x-ray beam was fixed but the beam energies are varied. So we conjecture that the conjugation planes of the P3HT and PCPDTBT must be locally orthogonal to each other.

The third component, $PC_{61}BM$, was taken into consideration. As seen in Figure 5a, without PCPDTBT, the thin film of P3HT-32k:$PC_{61}BM$ (0% PCPDTBT weight fraction) showed one scattering halo at q ~ 0.025 A^{-1}, corresponding to a d-spacing of ~25 nm. After blending a small amount of PCPDTBT to the thin film, e.g. 5% by weight, the scattering at q ~ 0.01 A^{-1} dominated, which corresponds to the average mesh size of ~60 nm consistent with the fibrillar network observed by TEM. The shoulder at q ~ 0.025 A^{-1} remained, which can be assigned to the fibril-fibril or nanocrystal-nanocrystal separation distance within the bundles. The primary scattering peak shifted to lower q and its intensity increased with the increasing PCPDTBT concentration; the corresponding domain sizes matched well with the mesh sizes in the TEM images. While the secondary peak at q ~ 0.025 A^{-1} was still visible. If the concentration of PCPDTBT exceeded 50%, only a weak, monotonically decreasing scattering was observed, indicating a uniform mixture. (Figure S6) Given the immiscibility of P3HT and PCPDTBT, these results indicate that $PC_{61}BM$ acts to solubilize both components.

Although it has already been shown that P3HT crystallized and that phase separation occurred in both P3HT:PCBM and the ternary blend thin films, it is surprising that the shape of the scattering pattern changed completely. P3HT-32k:PCBM showed an almost isotropic scattering pattern in

the tested range of 283.4 eV to 287 eV (Figure 5c,d); while anisotropic scattering patterns were observed for the ternary blend with 25% PCPDTBT and the direction of enhancement varied with the beam energies. (Figure 5e-h) Again, the sample itself was isotropic and the direction of the intensity enhancement for the scattering patterns was dependent on the x-ray polarization direction. (Figure S4) This implies that PCPDTBT influenced the orientation and ordering of the P3HT chains.

The data presented support an argument that P3HT crystallizes in a manner that was previously described by Strobl for a wide range of flexible polymers.[33-35] Upon spin coating, the polymers and PCBM are kinetically trapped in a mixed state. For P3HT:PCBM thin film, when thermal annealing was applied, P3HT initially nucleate with a random orientation of the crystals. With time, these unoriented P3HT nanocrystals were linked together to form the interpenetrating domains of P3HT fibrils. The scattering arising from this morphology would be independent of the polarization direction of the x-ray beam.

In the case of the ternary blend, P3HT and PCPDTBT are immiscible, which confines the nucleation and crystallization of the P3HT. The P3HT nanocrystals were aligned along the (010) direction due to the strong π-π stacking interactions. The fibrils were formed with the conjugated plane perpendicular to the long axis of the fibril. (Figure 5b) With 285.4 eV horizontally polarized x-rays, horizontally aligned transition dipole moments of P3HT, or, the P3HT fibrils with horizontal long axis, were highlighted. This would give rise to an anisotropic scattering profile with lobes of scattering along the vertical with a maximum characteristic of the mesh size of the network. With 284 eV x-rays, at the absorption edge characteristic of PCPDTBT, the

scattering pattern was found to be enhanced horizontally. This can only be explained if the conjugated plane of PCPDTBT is oriented, on average, orthogonal to that of P3HT. Since PCPDTBT is amorphous and mixed with PCBM and remaining amorphous P3HT in the interfibrillar areas, the maximum in the scattering appeared at the same scattering as that for P3HT.

A close examination of the TEM images for P3HT fibrils (Figure 2) in this study and some other studies reported show a granularity of the fibrillar structures, which is consistent with the association of nanocrystals.[34] The modulations in the fibrils in P3HT-32k:PCBM film were relatively large. With increasing PCPDTBT concentration, the confinement of PCPDTBT on P3HT became greater, so the fibrillar structure became better defined and the nanocrystals within the fibrils showed the better orientation. The fibrillar structures were clearer and the fibrils grew longer in TEM images and the variations between the horizontal and vertical directions in the scattering patterns became more pronounced. (Figure S7).

The evolution of the morphology was monitored as a function of thermal annealing time to clarify the driving force for the generation of the multi-length-scale morphology. GIXD profiles for the ternary blend with 25% PCPDTBT and P3HT-32k:$PC_{61}BM$ reference showed that the crystallization of P3HT is rapid in both cases. (Figure S8) Although the as-spun ternary blend film did not show any P3HT diffraction peaks and such peaks were evident for the as-spun P3HT-32k:PCBM film, after 30 s annealing or even longer, the peak position remained constant and crystal sizes were roughly the same. However, the development of the average domain size was different for the ternary blend and the binary reference.

As seen in the P-RSoXS profiles (Figure 6) for P3HT-32k:$PC_{61}BM$, intensity of the peak increased significantly after 30 s of annealing and shifted to a smaller q with a characteristic spacing of ~25 nm. Subsequent annealing for up to 2 h did not change the scattering significantly. For the ternary blend, the as-spun film showed a weak and monotonically deceasing scattering profile, indicating a uniform mixing of the three components. After 30 s of annealing, a broad shoulder is observed with a spacing corresponding to several of tens of nanometers. After 180 s of annealing, the two scattering peaks are clearly evident, where the primary peak corresponds to the mesh size of the network of P3HT fibrils. This reflection gradually shifted to the lower q and increased in intensity with longer annealing times. The secondary peak, with a characteristic distance of ~25 nm, corresponding to the fibril-fibril or nanocrystal-nanocrystal separation distance, remained unchanged with different annealing time. In addition, all the scattering patterns for the annealed ternary blend were anisotropic, indicating that the confinement of PCPDTBT starts from the beginning of P3HT crystal growth. The development of the domains is also evident in the TEM images (Figure S9). The morphology for P3HT-32k:$PC_{61}BM$ reference did not change much after thermal annealing. As for the ternary blend thin films, an increasing number of fibrils is seen with the increasing thermal annealing time and a better defined network of fibril bundles is seen after 180 s of annealing.

For thin film of P3HT:PCBM, the rapid crystallization of P3HT is the driving force for phase separation. $PC_{61}BM$ has a rapid diffusion rate at 150 ^{o}C and is excluded from the P3HT crystalline region.[26,36] Consequently, the evolution of the morphology of P3HT:$PC_{61}BM$ is quite fast and the P3HT crystallites are linked together with random orientation. With the addition of a

small amount of PCPDTBT (~25% weight fraction), crystallization of P3HT is one of the driving forces. This is coupled with the inherent phase separation between P3HT and PCPDTBT that put the confinement on the P3HT crystallization to form long fibrils with oriented crystal blocks and promote the further segregation to generate the network of fibril bundles and PCPDTBT/PCBM-rich amorphous region. The slow dynamics of domain growth and purification also indicated that the morphology of ternary blend was kinetically controlled.

It is well known that the crystallinity of P3HT and its miscibility with PCBM depend on its molecular weight.[37-39] Therefore, two other P3HTs with different molecular weights and PDI values were used to manipulate the morphology of the ternary blend. As shown in Figure 7a, the ternary blend of P3HT-28k:PCPDTBT:$PC_{61}BM$ (weight ratio of 3/1/4) displayed the typical network of fibril networks as that found with the ternary blend using P3HT-32k. But in the case of P3HT-28k, the fibrils were shorter and the mesh size of the network was smaller. As for the ternary blend using P3HT-19k, a few fibrils were observed; the fibrils were longer, but the network structure was not well-defined (Figure 7b).

The P-RSoXS profiles supported TEM images. The ternary using P3HT-28k showed the anisotropic scattering pattern by varying beam energy; and the direction of enhancement was the same as for the ternary blend using P3HT-32k. As for the ternary blend using P3HT-19k, the scattered intensities were too weak to quantitatively describe any anisotropies in the scattering profiles. To compare the domain size, the circularly averaged scattering profiles are plotted in Figure 7c. The scattering from P3HT-28k:PCPDTBT:$PC_{61}BM$ showed an intense reflection at q ~ 0.0068 A^{-1}, corresponding to the network mesh size of ~90 nm, and the shoulder at q ~ 0.025

A^{-1}, which was at the position as observed for the ternary blend using P3HT-32k. For the ternary blend using P3HT-19k, only a diffuse maximum was observed at low q, indicating a loss of the multi-scale length morphology.

Taken together, the variation of the device performance can be clearly explained by the evolution of the morphology. The dynamics of domain growth and purification are consistent well with the improvement of device performance as a function of thermal annealing time. As shown in Table S1, due to the rapid morphology evolution, the J_{sc} or PCE for P3HT-32k:PCBM solar cell increased rapidly after 30 s of thermal annealing, then continued to increase slightly, reaching a maximum after 30 m of annealing. While the J_{sc} or PCE for the ternary blend solar cell using P3HT-32k increased gradually within 3 minutes.

After being annealed for at least 3 minutes, a network of fibril bundles was generated. The ternary blend solar cell mimics a tandem cell connected in parallel. Bundles of P3HT fibrils with PCBM and/or amorphous PCPDTBT filling in the gaps could be considered as one kind of the "sub-cell"; while another kind of "sub-cell" is the amorphous region mainly containing PCPDTB:PCBM and, most likely, some amorphous P3HT. Since the domain sizes were comparable with the thickness of the active layer, these "sub-cells" can be thought to have roughly the same thickness and share the same electrodes. Therefore, the spectroscopic response was extended into a broader range of the solar spectrum, and the resultant J_{sc} value would be the sum of the J_{sc}s of the individual sub-cells. Furthermore, some PCPDTBT chains must stay at the interface between the P3HT fibrils and the amorphous region, suggested by their confinement on P3HT crystallization. This acts as a photosensitizer that bridges the charge transfer between

P3HT and PCBM efficiently, as reported by Koppe et al.[12] Both of the above two factors lead to the greater J_{sc} values relative to the P3HT-32k:$PC_{61}BM$ references. (Table S1) We also want to point out that, the smaller the network mesh size is, the larger the interfacial area; and the more PCPDTBT chains stay at the interface, the more efficient cascade charge transfer will be. As a result, for the ternary blend solar cell using P3HT-28k, which showed the smaller network mesh size, the great gain of J_{sc} overcompensated the loss of FF, resulting in ~27% increase of the device efficiency relative to the binary reference after 10 m annealing. (Table S2) While for the ternary cell using P3HT-32k, the gain in J_{sc} could not compensate the loss in FF, leading to the slightly lower PCE compared with P3HT-32k:PCBM cell. (Table S1)

In addition, the morphology of the ternary blend showed better stability compared to the P3HT: $PC_{61}BM$ reference. Large $PC_{61}BM$ aggregations could be observed by optical microscopy (OM) for the P3HT-32k:$PC_{61}BM$ thin film after 2 h of thermal annealing (Figure S10), so the J_{sc} for P3HT-32k:$PC_{61}BM$ cell decreased slightly. While no aggregation of the $PC_{61}BM$ formed for the ternary blend thin film because of the slow domain development and the miscibility of PCPDTBT with $PC_{61}BM$ in the amorphous region. Therefore, the J_{sc} for the ternary blend cell using P3HT-32k continued to increase. Finally, the gain in J_{sc} was greater than the drop in the FF, resulting in an efficiency that was higher than the binary references.

As for the ternary blend solar cells using P3HT-19k with 25% weight fraction of PCPDTBT in total polymers, or those using P3HT-32k with higher contents of PCPDTBT larger than 50% weight fraction, the crystallinity of P3HT was suppressed, the percolation network of P3HT

fibrils was lost and the three components intimately mixed. Consequently, charge recombination became serious and the device performance deteriorated as seen in Table S2 and S3.

4. Conclusion

In summary, we have shown that a multi-length-scale morphology formed for ternary blends P3HT:PCPDTBT:$PC_{61}BM$ by controlling the blending ratio, thermal annealing time and P3HT molecular weight. With the suitable molecular weight of P3HT, the addition of a small amount of amorphous PCPDTBT preserves the high crystallinity of P3HT; and well-defined P3HT fibrils were formed rapidly under confinement with a certain orientation due to the immiscibility between P3HT and PCPDTBT. These fibrils were segregated from the amorphous region and generated the bundles. Thus, the ternary blend solar cells can be considered as a combination of two distinct sub-cells connected in parallel, where one sub-cell is rich in P3HT fribrils and another rich in PCPDTBT with other amorphous part. The photoresponse of such ternary cells covers a broad range of the solar spectra and parallel-like charge transfer exists. In addition, PCPDTBT at the interface of the crystal act as a photosensitizer to benefit the cascade charge transfer. The two donor polymers worked independently and even synergistically to achieve the better device performance relative to the binary references.

Acknowledgements

This work was supported by the Department of Energy supported Energy Frontier Research Center at the University of Massachusetts under contract DE-SC0001087. We thank Anthony Young for assisting P-RSoXS measurements at 11.0.1.2, ALS, LBNL. Portions of this research

were carried out and supported by the Advanced Light Source, Lawrence Berkeley National Laboratory, which was supported by the DOE, Office of Science, and Office of Basic Energy Sciences. A portion of this research was conducted at the Center for Nanophase Materials Sciences, which is sponsored at Oak Ridge National Laboratory by the Division of Scientific User Facilities, Office of Basic Energy Sciences, U.S. Department of Energy. We also thank Kurashiki Research Center in Kuraray Co. Ltd, Japan, for providing P3HT-28k.

Notes and References

1 A. Hadipour, B. de Boer, P. W. M. Blom, *Adv. Funct. Mater.* 2008, **18**, 169.

2 L. Dou, J. You, J. Yang, C. Chen, Y. He, S. Murase, T. Moriarty, K. Emery, G. Li, Y. Yang, *Nat. Photon.* 2012, **6**, 180.

3 J. Y. Kim, K. Lee, N. E. Coates, D. Moses, T. Nguyen, M. Dante, A. J. Heeger, *Science* 2007, **317**, 222.

4 PRESS RELEASE. www.heliatek.com.

5 S. Sista, Z. Hong, L. Chen, Y. Yang, *Energy Environ. Sci.* 2011, **4**, 1606.

6 Y. Yuan, J. Huang, G. Li, *Green* 2011, **1**, 65–80.

7 G. Dennler, K. Forberich, T. Ameri, C. Waldauf, P. Denk, C. J. Brabec, K. Hingerl, A. J. Heeger, *J. Appl. Phys.* 2007, **102**, 123109.

8 G. Namkoong, P. Boland, K. Lee, J. Dean, *J. Appl. Phys.* 2010, **107**, 124515.

9 T. Ameri, P. Khoram, J. Min, C. J. Brabec, *Adv. Mater.* 2013, **25**, 4245.

10 Y. Chen, C. Hsu, R. Y. Lin, K. Ho, J. T. Lin, *ChemSusChem* 2013, **6**, 20.

11 T. Ameri, J. Min, N. Li, F. Machui, D. Baran, M. Forster, K. J. Schottler, D. Dolfen, U. Scherf, C. J. Brabec, *Adv. Energy Mater.* 2012, **2**, 1198.

12 M. Koppe, H. J. Egelhaaf, G. Dennler, M. C. Scharber, C. J. Brabec, P. Schilinsky, C. N. Hoth, *Adv. Funct. Mater.* 2010, **20**, 338.

13 Z. Hu, S. Tang, A. Ahlvers, S. I. Khondaker, A. Gesquiere, *J. Appl. Phys. Lett.* 2012, **101**, 053308.

14 L. Yang, H. Zhou, S. C. Price, W. You, *J. Am. Chem. Soc.* 2012, **134**, 5432.

15 P. P. Khlyabich, B. Burkhart, B. C. Thompson, *J. Am. Chem. Soc.* 2012, **134**, 9074.

16 F. Machui, S. Rathgeber, N. Li, T. Ameri, C. J. Brabec, *J. Mater. Chem.* 2012, **22**, 15570.

17 H. Kim, M. Shin, Y. Kim, *J. Phys. Chem. C* 2009, **113**, 1620.

18 M. C. Chen, D. J. Liaw, Y. C. Huang, H. Y. Wu, Y. Tai, *Sol. Energy Mater. Sol. Cells* 2011, **95**, 2621.

19 N. Li, F. Machui, D. Waller, M. Koppe, C. J. Brabec, *Sol. Energy Mater. Sol. Cells* 2011, **95**, 3465.

20 I. Osaka, R. D. McCullough, *Acc. Chem. Res.* 2008, **41**, 1202.

21 E. Gann, A. T. Young, B. A. Collins, H. Yan, J. Nasiatka, H. A. Padmore, H. Ade, A. Hexemer, C. Wang, *Rev. Sci. Instrum.* 2012, **83**, 045110.

22 M. Aryal, K. Trivedi, W. Hu, *ACS Nano* 2009, **3**, 3085.

23 S. Lilliu, T. Agostinelli, E. Pires, M. Hampton, J. Nelson, J. E. Macdonald, *Macromolecules* 2011, **44**, 2725.

24 M. Y. Chiu, U. S. Jeng, M. S. Su, K. H. Wei, *Macromolecules* 2010, **43**, 428.

25 Y. Gu, C. Wang, T. P. Russell, *Adv. Energy Mater.* 2012, **2**, 683.

26 D. Chen, A. Nakahara, D. Wei, D. Nordlund, T. P. Russell, *Nano Lett.* 2011, **11**, 561.

27 J. T. Rogers, K. Schmidt, M. F. Toney, E. J. Kramer, G. C. Bazan, *Adv. Mater.* 2011, **23**, 2284.

28 T. Agostinelli, T. A. M. Ferenczi, E. Pires, S. Foster, A. Maurano, C. Muller, A. Ballantyne, M. Hampton, S. Lilliu, M. Campoy-Quiles, H. Azimi, M. Morana, D. D. C. Bradley, J. Durrant, J. E. Macdonald, N. Stingelin, J. Nelson, *J. Polym. Sci., Part B: Polym. Phys.* 2011, **49**, 717.

29 L. F. Drummy, R. J. Davis, D. L. Moore, M. Durstock, R. A. Vaia, J. W. P. Hsu, *Chem. Mater.* 2011, **23**, 907.

30 C. Wang, A. Hexemer, J. Nasiatka, E. R. Chan, A. T. Young, H. A. Padmore, W. F. Schlotter, J. Lüning, S. Swaraj, B. Watts, E. Gann, H. Yan, H. Ade, *IOP Conf. Ser.: Mater. Sci. Eng.* 2010, **14**, 012016.

31 B. A. Collins, J. E. Cochran, H. Yan, E. Gann, C. Hub, R. Fink, C. Wang, T. Schuettfort, C. R. McNeill, M. L. Chabinyc, H. Ade, *Nat. Mater.* 2012, **11**, 536.

32 D. M. DeLongchamp, B. M. Vogel, Y. Jung, M. C. Gurau, C. A. Richter, O. A. Kirillov, J. Obrzut, D. A. Fischer, S. Sambasivan, L. J. Richter, E. K. Lin, *Chem. Mater.* 2005, **17**, 5610.

33 G. Strobl, *Eur. Phys. J. E* 2000, **3**, 165.

34 T. Hugel, G. Strobl, R. Thomann, *Acta. Polym.* 1999, **50**, 214.

35 J. Loos, P.C. Thune, J. W. Niemantsverdriet, P. J. Lemstra, *Macromolecules* 1999, **32**, 8910.

36 N. D. Treat, M. A. Brady, G. Smith, M. F. Toney, E. J. Kramer, C. J. Hawker, M. L. Chabinyc, *Adv. Energy Mater.* 2010, **1**, 82.

37 M. Brinkmann, P. Rannou, *Macromolecules* 2009, **42**, 1125.

38 C. Nicolet, D. Deribew, C. Renaud, G. Fleury, C. Brochon, E. Cloutet, L. Vignau, G. Wantz, H. Cramail, M. Geoghegan, G. Hadziioannou, *J. Phys. Chem. B* 2011, **115**, 12717.

39 F. P. V. Koch, J. Rivnay, S. Foster, C. Muller, J. M. Downing, E. Buchaca-Domingo, P. Westacott, L. Yu, M. Yuan, M. Baklar, Z. Fei, C. Luscombe, M. A. McLachlan, M. Heeney, G. Rumbles, C. Silva, A. Salleo, J. Nelson, P. Smith, N. Stingelin, *Prog. Polym. Sci.* 2013, **38**, 1978.

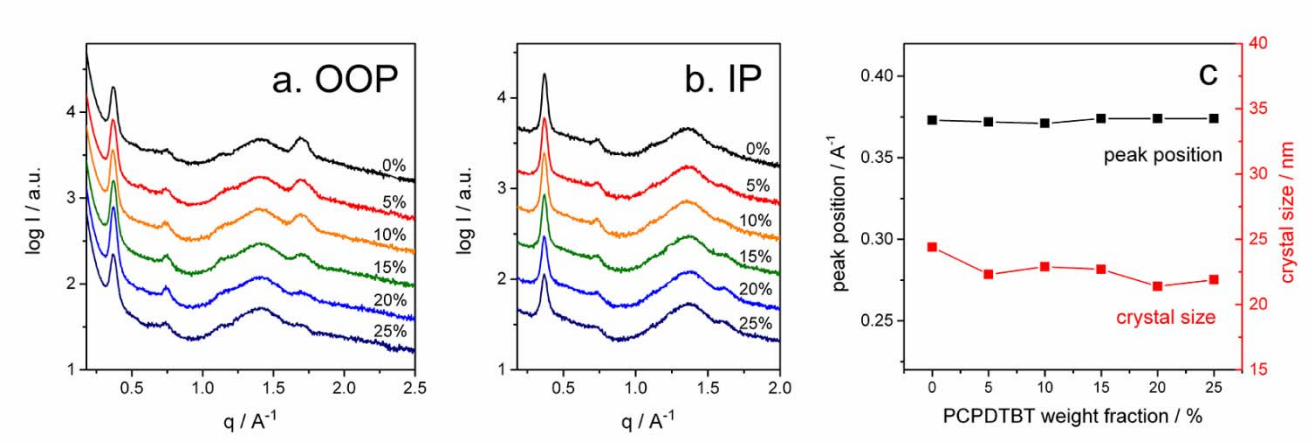

Figure 1. GIXD (a) OOP or (b) IP profiles for P3HT-32k:PCPDTBT:$PC_{61}BM$ ternary blend thin films with different PCPDTBT weight fraction in total polymers. (c) summary for the P3HT OOP (100) peak position and the estimated crystal size.

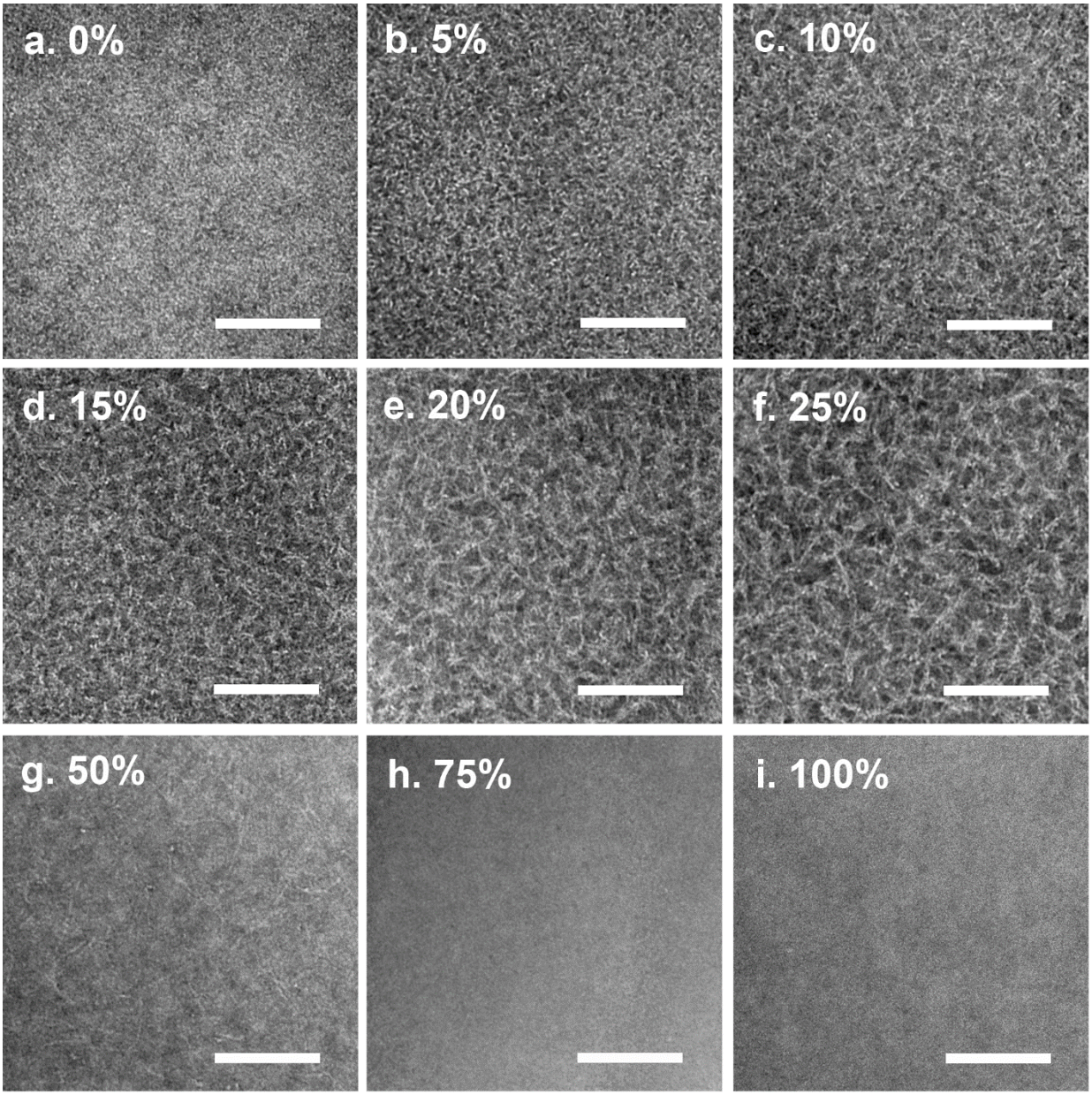

Figure 2. BF-TEM images for ternary blend thin films using P3HT-32k with different PCPDTBT contents. The weight ratio of polymer to PCBM was kept to be 1. The labeled number is the weight fraction of PCPDTBT in total polymers. The scale bar is 500 nm.

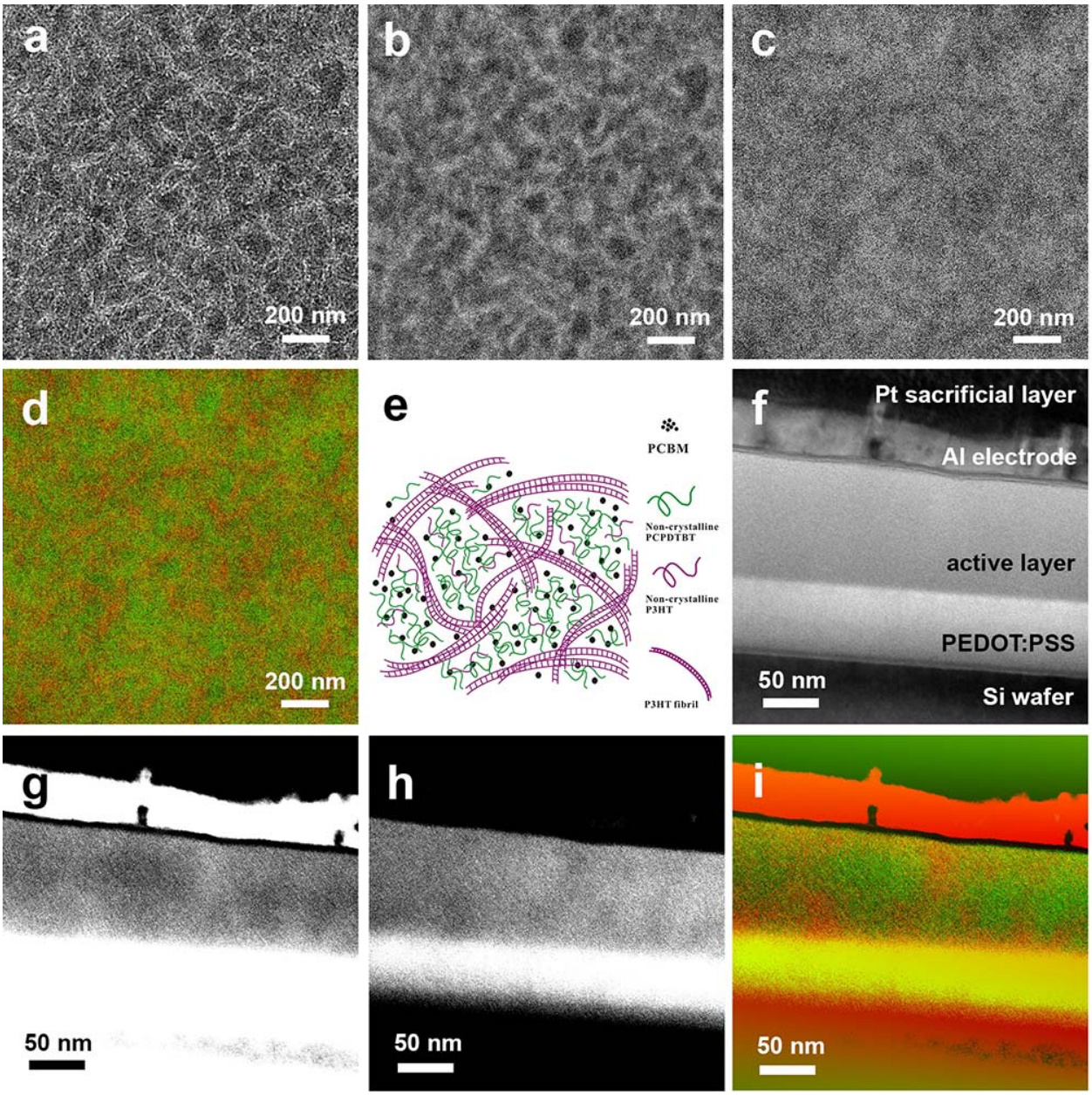

Figure 3. EF-TEM (a) 0±4 eV, (b) 19±4 eV, (c) 30±4 eV images, (d) color mix map for lateral section of pre-annealed ternary blend thin films of P3HT-32k:PCPDTBT:PCBM with weight ratio of 3/1/4 (25 wt% of PCPDTBT) and the corresponding scheme (e). EF-TEM (f) 0±4 eV, (g) 19±4 eV, (h) 30±4 eV images, (i) color mix map for cross-section of post-annealed ternary blend thin films of P3HT-32k:PCPDTBT:PCBM with weight ratio of 3/1/4.

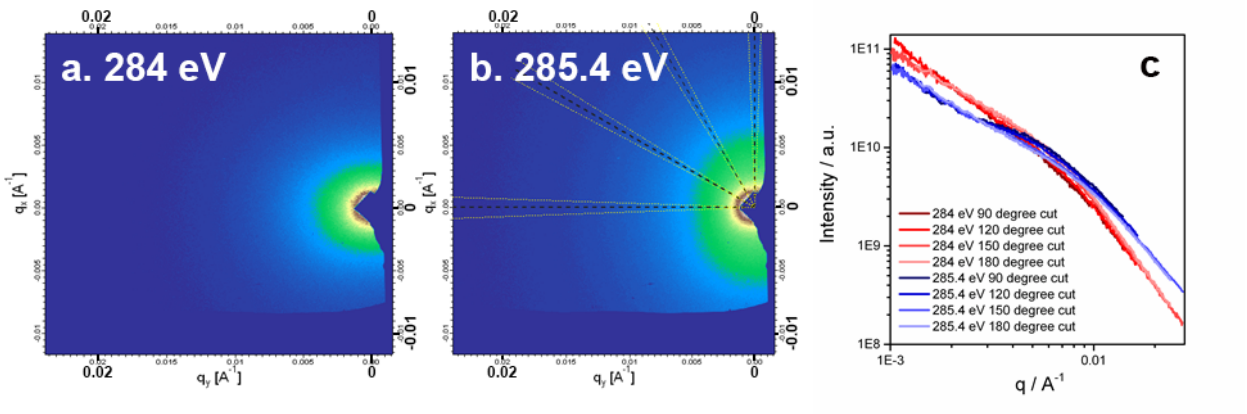

Figure 4. P-RSoXS patterns (a, b) and sector averaged profiles (c) for P3HT-32k:PCPDTBT thin film (3/1 wt/wt, spin-coated by CB, post-annealed) with horizontally polarized x-ray beam.

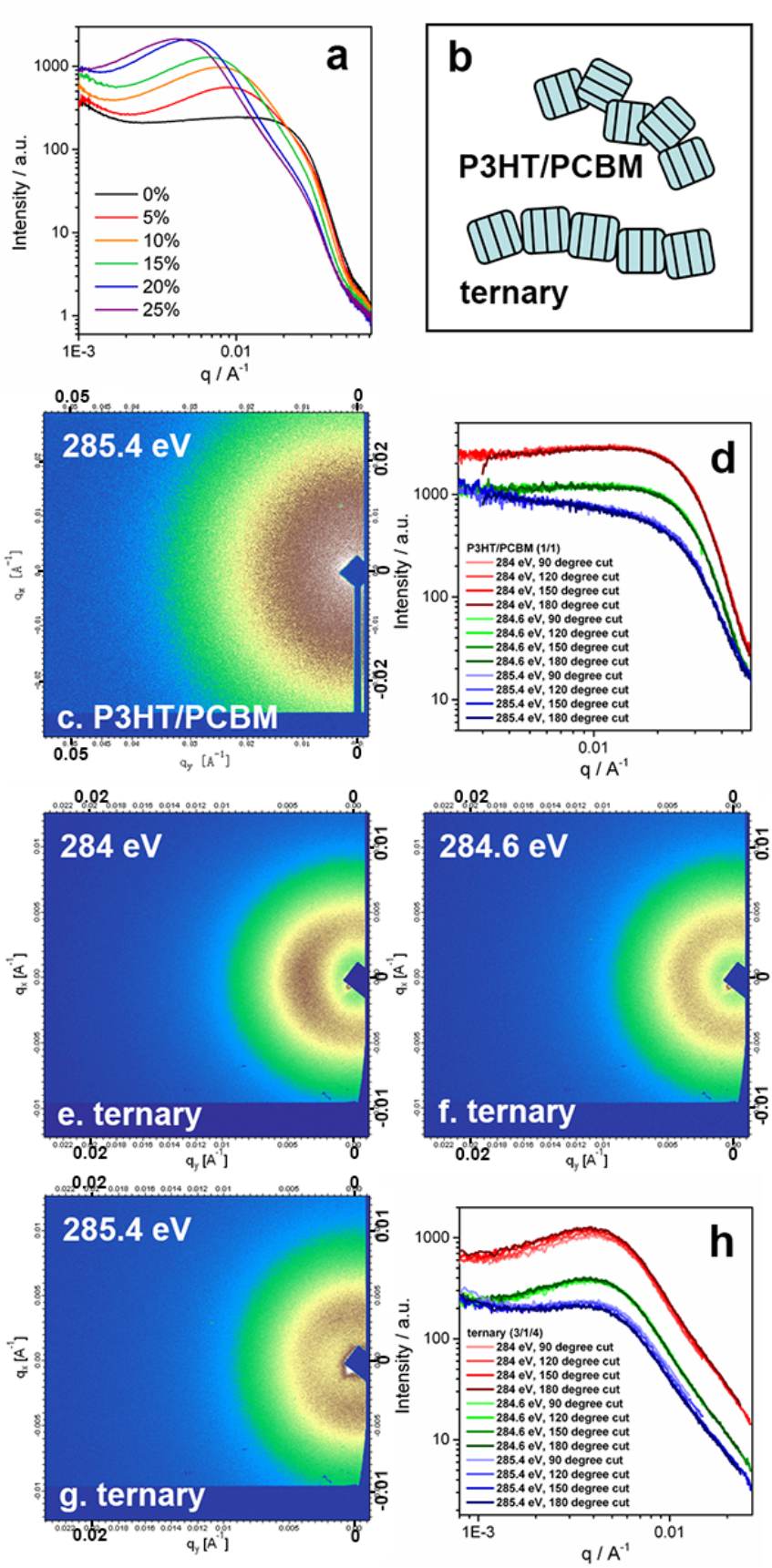

Figure 5. (a) P-RSoXS circularly averaged profiles for ternary blend thin film using P3HT-32k with different PCPDTBT contents at 284 eV horizontally polarized x-ray beam. (b) Scheme for the orientation of P3HT nanocrystals within the fibrils in thin films of P3HT:PCBM or the ternary blend. P-RSoXS pattern and sector averaged profiles for post-annealed thin film of P3HT:PCBM (1/1) (c,d) or ternary blend (3/1/4) (e-h) using P3HT-32k at horizontally polarized x-ray beam.

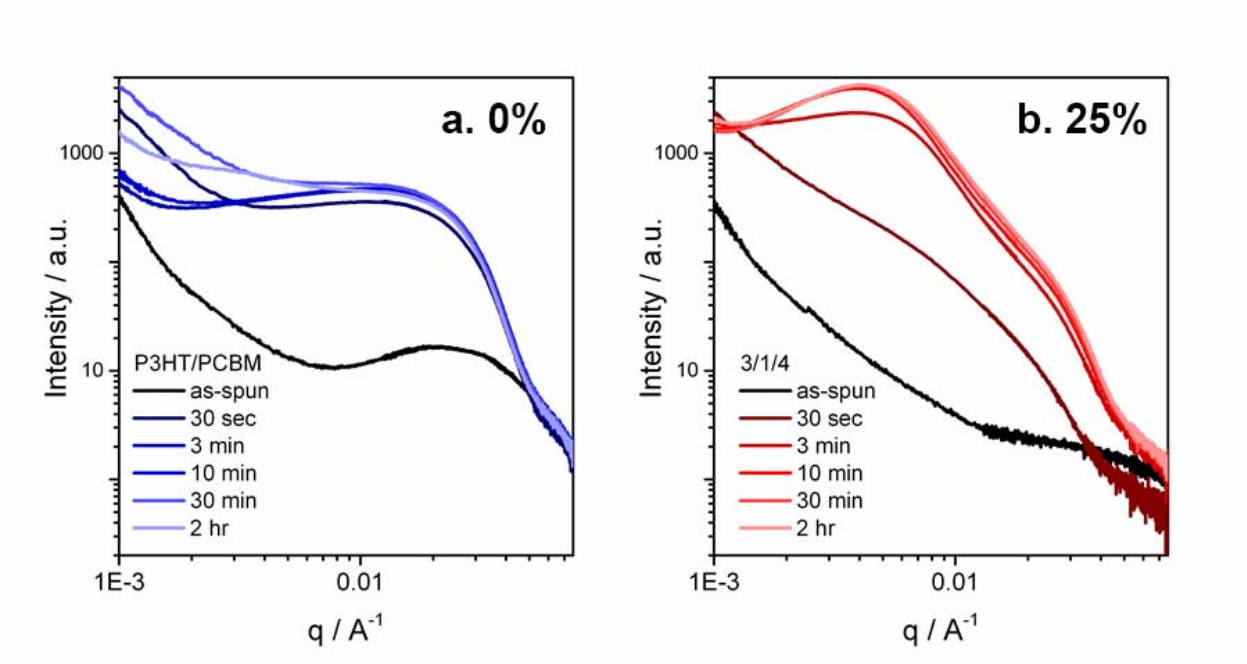

Figure 6. P-RSoXS circularly averaged profiles (284 eV, horizontally polarized x-ray beam) for thin films of P3HT-32k:PCBM (1/1) (a) and P3HT-32k:PCPDTBT:PCBM (3/1/4) (b) spin-coated by CB and post-annealed for a different time.

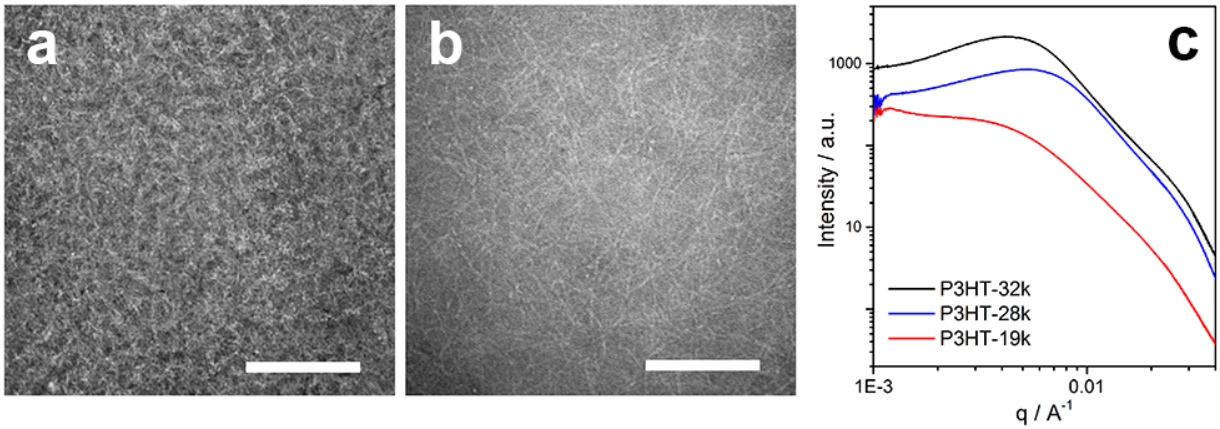

Figure 7. BF-TEM images for thin films of P3HT-28k:PCPDTBT:PCBM (a) and P3HT-19k:PCPDTBT:PCBM (b) with the weight ratio of 3/1/4. The scale bar is 500 nm. (c) P-RSoXS circularly averaged profiles (284 eV, horizontally polarized x-ray beam) for the ternary blend thin films using different molecular weights of P3HT. The curves were shifted vertically.